energies

MDPI

Article

Time-Multiplexed Self-Powered Wireless Current Sensor for Power Transmission Lines

Hao Chen, Zhongnan Qian, Chengyin Liu, Jiande Wu *, Wuhua Li and Xiangning He

College of Electrical Engineering, Zhejiang University, Hangzhou 310027, China; 21910045@zju.edu.cn (H.C.); zhongnanqian_ee@zju.edu.cn (Z.Q.); 3170102374@zju.edu.cn (C.L.); woohualee@zju.edu.cn (W.L.); hxn@zju.edu.cn (X.H.)

* Correspondence: eewjd@zju.edu.cn; Tel.: +86-1360-051-1674

Abstract: Current measurement is a key part of the monitoring system for power transmission lines. Compared with the conventional current sensor, the distributed, self-powered and contactless current sensor has great advantages of safety and reliability. By integrating the current sensing function and the energy harvesting function of current transformer (CT), a time-multiplexed self-powered wireless sensor that can measure the power transmission line current is presented in this paper. Two operating modes of CT, including current sensing mode and energy harvesting mode, are analyzed in detail. Through the design of mode-switching circuit, harvesting circuit and measurement circuit are isolated using only one CT secondary coil, which eliminates the interference between energy harvesting and current measurement. Thus, the accurate measurement in the current sensing mode and the maximum energy collection in the energy harvesting mode are both realized, all of which simplify the online power transmission line monitoring. The designed time-multiplexed working mode allows the sensor to work at a lower transmission line current, at the expense of a lower working frequency. Finally, the proposed sensor is verified by experiments.

Keywords: time-multiplexed; self-powered; current transformer; current sensor

Citation: Chen, H.; Qian, Z.; Liu, C.; Wu, J.; Li, W.; He, X. Time-Multiplexed Self-Powered Wireless Current Sensor for Power Transmission Lines. *Energies* **2021**, *14*, 1561. https://doi.org/10.3390/en14061561

Academic Editor: Salvatore Celozzi

Received: 4 February 2021
Accepted: 8 March 2021
Published: 11 March 2021

1. Introduction

Power transmission and distribution networks has high requirements for reliability and security, and a reliable online condition monitoring system (OCMS) can provide the guarantees [1]. Meanwhile, OCMS is also a prerequisite for the development of smart grid [2,3]. New technologies of smart grid, such as dynamic line rating [4] and situation awareness [5], require wide-area line operation data based on widely distributed OCMS. In the OCMS for power transmission lines, line current measurement can directly reflect the operation status of transmission lines and different line faults [6]. Therefore, line current measurement is an intuitive way of OCMS for power transmission lines [7].

Lots of distributed current sensors are required for online current measurements. Due to the high voltage and high current of power transmission lines, direct electrical contact between sensors and transmission lines is dangerous. Thus, non-contact current measurement methods for electric power systems have been developed, such as current transformer (CT), Rogowski coil [8], Hall current sensor [9], fluxgate and optical current sensor [10], etc. Among them, the CT is widely adopted. The line-clamped CT transforms the large power transmission line current to a small current on the secondary side, which is safe to measure.

Besides, the power supply technology for distributed current sensors on power transmission lines is also a challenge. To overcome the battery replacement issue, energy harvesting methods have been widely studied for this application, including electromagnetic coupling, thermal [11], solar [12], and wind [13]. Solar and wind power are highly dependent on weather conditions, so the energy storage element is bulky for continuous power supply, which is undesirable on transmission lines. Thermal harvesters are also unstable for transmission line applications due to the wide temperature swing between transmission lines and ambient environments. Compared to them, the CT-fed power supply, a kind of magnetic coupling method, is more suitable for transmission line applications [14]. Since energy is sourced from the transmission lines by CT, the power supply can be constantly maintained to ensure the uninterrupted operation of sensors.

Therefore, the line-clamped CT can be used for both current sensing and energy harvesting, which depends on different post-stage circuit designs. To simplify the OCMS structure, self-powered current sensors that combine the functions of current sensing and energy harvesting are proposed in [15–18]. Amaro et al. [15] proposed a system that is capable of supplying power to a wireless sensor and at the same time estimating the line current. The energy sourced by CT is stored in a capacitor, and the current value is estimated by promoting capacitor discharge and estimating the slope of the recharging voltage. Ren et al. [16] presented a self-powered current measuring sensor realizing measurement and power supply synchronously. The current is calculated by the voltage and current before and after the rectifier connected to post-stage of CT. Neither of the aforementioned two methods isolates the measurement circuit from the harvesting circuit, which decreases the current measurement accuracy. Moghe et al. [17] proposed a smart stick-on sensor for monitoring a variety of grid assets. It is pointed out that the isolation between current measurement circuit and harvesting circuit can improve the measurement accuracy. However, the detailed isolated circuit design is not given. Lim et al. [18] proposed a CT structure with two secondary coils for self-powered current sensors, in which one coil is used for current sensing, and the other one is used for energy harvesting. Through this CT structure, the measurement circuit and the harvesting circuit are successfully isolated. However, as the cost of the integration of two secondary coils into one core, a voltage reduction in the energy storage capacitor is expected. Consequently, the sensor needs a higher line current to operate.

In this paper, a time-multiplexed self-powered wireless current sensor for transmission lines is proposed. The mode-switching circuit is designed to isolate the harvesting circuit and the measurement circuit, making the sensor work in time-multiplexed mode, which eliminates the interference between energy harvesting and current measurement. The accurate current measurement and the maximum energy collection are realized through only one CT secondary coil instead of two coils. Meanwhile, the time-multiplexed working mode allows the sensor to work at a lower transmission line current, at the expense of lower working frequency. The proposed sensor makes full use of the transducer and simplifies OCMS for power transmission lines.

This paper is organized as follows. In Section 2, the ideal and non-ideal models of CT are presented and analyzed. Based on the non-ideal model, the impedance matching of the post-stage circuit in both current sensing mode and energy harvesting mode is analyzed. In Section 3, the design of time-multiplexed self-powered wireless current sensor is proposed, and its workflow is analyzed in detail. In Section 4, experimental results are presented to verify the proposed sensor. In Section 5, the conclusions are given.

2. Analysis of CT Operating Modes

2.1. Circuit Model of CT

As shown in Figure 1, the CT is clamped on a single-phase AC transmission line, and the secondary side is connected to the load. The turn ratio of the primary and the secondary is 1:N. Assuming magnetic core works in linear region and neglecting nonideal factors of CT, an ideal circuit model of CT can be derived. According to the principle of magnetic potential balance, when the transmission line carries current $i_\mathrm{p}(\mathrm{t})$ (i.e., the primary side of CT), current $i_\mathrm{s}(\mathrm{t})$ will also be induced through the load (i.e., the secondary side of CT). The current relationship is:

$$i_\mathrm{L}(\mathrm{t}) = i_\mathrm{s}(\mathrm{t}) = i_\mathrm{p}(\mathrm{t})/N \tag{1}$$

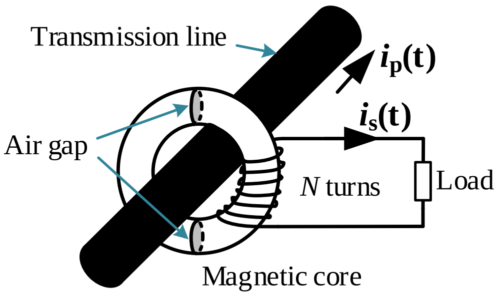

Figure 1. CT setup.

Thus, the ideal circuit model of CT is built, as shown in Figure 2.

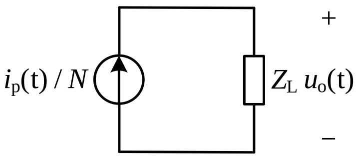

Figure 2. Ideal circuit model of CT.

Considering finite magnetizing inductance, flux leakage, core loss, and wire loss, a non-ideal model of CT can be built, as shown in Figure 3a. The magnetizing inductance L_m of CT has a certain shunting effect on the current source $i_p(t)/N$. Especially when the air gap is added in the core, the value of L_m will drop dramatically, and the shunting effect will be more noticeable, resulting in a much smaller current through the load than the ideal condition. In addition, the core loss of CT also has a significant influence on the load power, which is modeled by the resistance R_m. The leak inductance L_σ and the wire loss resistance R_w of the secondary winding are also non-ideal factors of practical CT. However, considering that the load impedance of the secondary side is typically much larger than the leak impedance, the leak impedance of the secondary side can be ignored. Accordingly, the simplified CT non-ideal circuit model can be derived, as shown in Figure 3b.

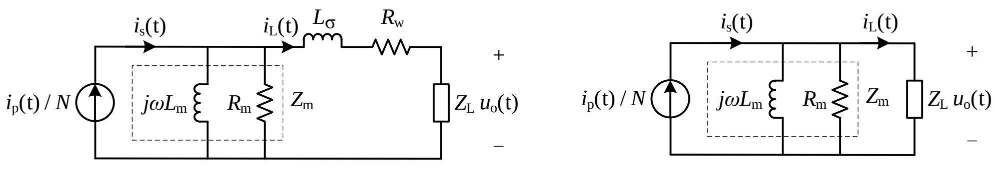

Figure 3. Non-ideal circuit model of CT. (**a**) With leak impedance. (**b**) Ignore leak impedance.

2.2. Current Sensing Mode of CT

When CT is utilized to sense the primary side current, assume that the CT is ideal, the secondary side current $i_s(t)$ completely through the load, as shown in Figure 2. Thus, the primary side current $i_p(t)$ can be calculated by Equation (1) after the current $i_s(t)$ is measured.

However, for the non-ideal CT model, as shown in Figure 3b, due to the shunting effect of L_m and R_m, the current through the load is smaller than the ideal condition. Thus, a measurement error would be produced if Equation (1) is used to calculate the primary current. In the non-ideal model shown in Figure 3b, the current through the load Z_L is:

$$i_L = \frac{i_p}{N} \cdot \frac{j\omega L_m + R_m}{j\omega L_m + R_m + Z_L} \tag{2}$$

Thus, the relative error of measurement is:

$$\delta = \left|1 - \frac{I_{\mathrm{L}}}{I_{\mathrm{s}}}\right| = \left|\frac{Z_{\mathrm{L}}}{j\omega L_{\mathrm{m}} + R_{\mathrm{m}} + Z_{\mathrm{L}}}\right| \tag{3}$$

Since L_{m} and R_{m} are determined, for minimizing the relative error, Z_{L} is expected to be much less than ($j\omega L_{\mathrm{m}}$ + R_{m}), which is the requirement that CT post-stage circuit needs to satisfy in the current sensing mode.

2.3. Energy Harvesting Mode of CT

When CT is utilized for energy harvesting, the load Z_{L} is expected to absorb power as much as possible. According to the circuit model shown in Figure 3b, the output power is:

$$P_{Z_{\mathrm{L}}} = \left|\frac{I_{\mathrm{p}}}{N} \times \frac{j\omega L_{\mathrm{m}} + R_{\mathrm{m}}}{j\omega L_{\mathrm{m}} + R_{\mathrm{m}} + Z_{\mathrm{L}}}\right|^2 \times Z_{\mathrm{L}} \tag{4}$$

In this mode, when the parameters of CT and the primary current are fixed, the CT output power is related to the impedance of the load. The conventional CT energy harvesting circuit directly connects the secondary side to a resistive load, as shown in Figure 4, without considering the compensation for CT magnetizing inductance L_{m} and impedance matching. The maximum output power of the harvester without compensation and with compensation will be analyzed and compared below.

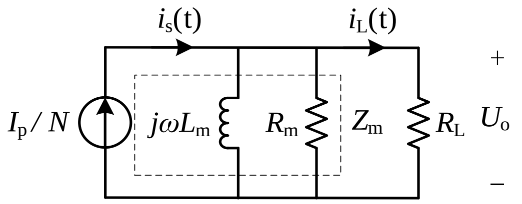

Figure 4. CT energy harvesting circuit without compensation.

In the case of no compensation, as shown in Figure 4, the parameters of CT and the primary current are fixed, and only R_{L} is variable. When R_{L} is set as:

$$R_{\mathrm{L}} = \frac{1}{\sqrt{\left(\frac{1}{R_{\mathrm{m}}}\right)^2 + \left(\frac{1}{\omega L_{\mathrm{m}}}\right)^2}} \tag{5}$$

The output power is maximized to:

$$P_{\mathrm{L1}} = \left(\frac{I_{\mathrm{p}}}{N}\right)^2 \cdot \frac{1}{2\left[\sqrt{\left(\frac{1}{R_{\mathrm{m}}}\right)^2 + \left(\frac{1}{\omega L_{\mathrm{m}}}\right)^2} + \frac{1}{R_{\mathrm{m}}}\right]} \tag{6}$$

The harvester with compensation is shown in Figure 5, a parallel capacitor C_{r} is utilized to compensate the magnetizing inductance L_{m}. According to the principle of impedance matching, when C_{r} and R_{L} satisfy Equation (7), the power absorbed by R_{L} is maximized.

$$\begin{cases} C_{\mathrm{r}} = \frac{1}{\omega^2 L_{\mathrm{m}}} \\ R_{\mathrm{L}} = R_{\mathrm{m}} \end{cases} \tag{7}$$

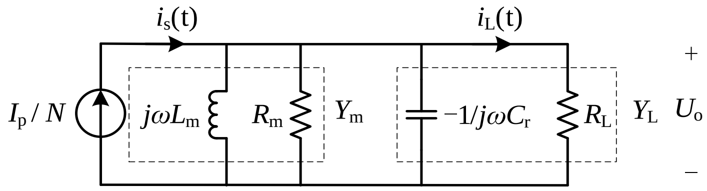

Figure 5. CT energy harvesting circuit with compensation capacitance.

In this case, the CT output power is:

$$P_{L2} = \left(\frac{I_p}{N}\right)^2 \cdot \frac{R_m}{4} \tag{8}$$

For the general case where the C_r matches L_m and the load R_L is variable, the CT output power is:

$$P_{L2} = \left(\frac{I_p}{N}\right)^2 \cdot \frac{R_m^2}{R_L + R_m^2/R_L + 2R_m} \tag{9}$$

Comparing Equations (6) and (9), the maximum harvesting power of CT is improved compared with that of without compensation, as shown in the following equation.

$$\frac{P_{L2}}{P_{L1}} = \frac{1}{2}\left[1 + \sqrt{1 + \left(\frac{R_m}{\omega L_m}\right)^2}\right] > 1 \tag{10}$$

Especially, when the air gap is added in the core, L_m is significantly decreased, yet R_m is almost unchanged (because there is no loss in the air gap), so the ratio of R_m to ωL_m is significantly increased. It can be seen from Equation (10) that, at this time, the CT output power will be significantly enhanced by paralleling the compensation capacitor on the secondary side of CT.

When the load of the harvester is a full-bridge rectifier with resistive load, as shown in Figure 6, the rectifier can be approximated to a resistive load to the harvester.

$$R_{L(eq)} \approx R_{rec}/2 \tag{11}$$

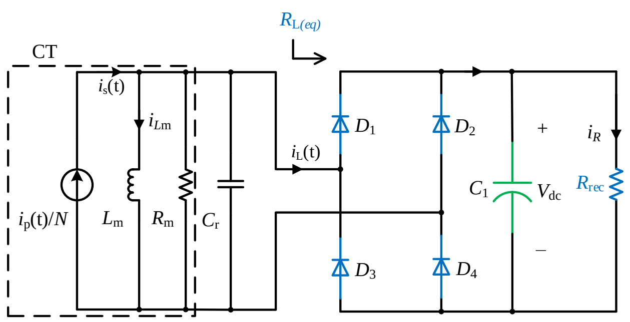

Figure 6. Full-bridge rectifier for CT energy harvester.

3. Design of Time-Multiplexed Self-Powered Wireless Current Sensor

3.1. System Structure and Circuit Design

The system structure of the proposed time-multiplexed self-powered wireless current sensor is shown in Figure 7. The CT of the sensor is clamped on the transmission line. The current sensing function and the energy harvesting function of CT are integrated into the sensor. The system has two operating modes, energy harvesting mode, and current measurement mode. The two modes are converted by mode switch.

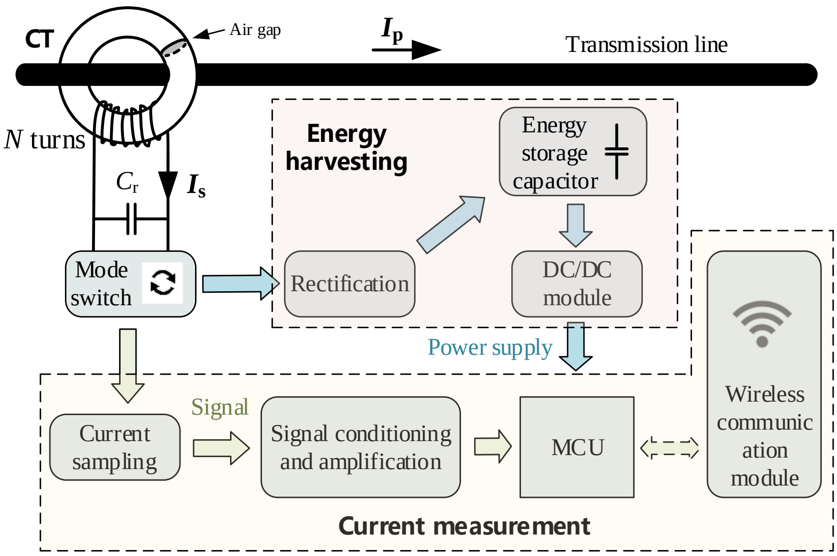

Figure 7. System structure of the time-multiplexed self-powered wireless current sensor.

In the energy harvesting mode, the energy sourced by CT from the transmission line is stored in an energy storage capacitor. When enough energy is stored, the system switches to the current measurement mode, and the measurement circuit is powered. The measurement circuit senses the CT secondary side current value, calculates the CT primary side current value, and finally sends the results via the wireless communication module to realize further function. When the stored energy is insufficient, the system switches the energy harvesting mode, and the cycle repeats. Thus, the harvesting circuit and the measurement circuit are isolated by the mode switch, and the sensor is time-multiplexed, which eliminates the interference between energy harvesting and current measurement. Compared with the method using two CT secondary coils, the proposed sensor realizes the isolation between the harvesting circuit and the measurement circuit using only one CT secondary coil.

The current range of transmission lines needs to be considered in the implementation of the current sensor. When the transmission line current is low, the traditional CT harvester may not be able to source enough energy to maintain a stable DC voltage to power the post-stage circuit. Due to the wide dynamic current range of the transmission line, an energy storage device is necessary. On the other side, for the distributed wireless current sensor, one of the most critical challenges is to achieve optimum operational life. Compared to a lithium battery with a short life span [19], the electrolytic capacitor has extremely high cycle life and operates with unexcelled reliability [20]. Accordingly, the high-capacity electrolytic capacitor C_1 is used as an energy storage device in the proposed sensor. The sensor works in time-multiplexed mode, the working frequency of the sensor varies with the transmission line current. By extending the time operating in energy harvesting mode, it can adapt itself to a low current condition, at the expense of a lower operating frequency. The sensor can operate at a minimum transmission line current of 1 A.

Accurate transmission line current measurement needs to ensure the effectiveness of Equation (1). In other words, the primary current of the CT has a linear relationship with the secondary current under the utility-frequency condition. To ensure the linear relationship, the magnetic core of CT needs to operate in a linear region to prevent the effects of loss and magnetic saturation, because saturation will cause secondary current distortion [21]. Thus, an air gap is added in the core to expand the unsaturated operating range, as shown in Figure 7, making the linear region of the core cover the maximum current range.

The parameters and dimensions of CT need to consider the scale and power level of the transmission line. Considering the saturation of the magnetic core and the accuracy of current measurement, a single CT cannot satisfy the needs of a wide range of current measurements. Different CT can be chosen to satisfy the needs of the sensor operating in different current ranges of the transmission line. Since the proposed sensor can operate at a minimum transmission line current of 1 A, the CT with an operating current range of 1–100 A is chosen. Thus, the current measurement range of the proposed sensor is 1–100 A.

The detailed circuit of the proposed time-multiplexed self-powered wireless current sensor is shown in Figure 8. The circuit consists of three parts, energy harvesting part, current measurement part, and mode switch part. The energy harvesting part includes the CT, the compensation capacitor C_r, the full-bridge rectifier (composed of diodes D_1, D_2, and body diodes of Q_3 and Q_4), and the energy storage capacitor C_1. The current measurement part is composed of sample resister R_1 and R_2, differential amplification module, microprogrammed control unit (MCU), MOSFET driver, and the LoRa (Long Range Radio) wireless communication module, where the R_1 and R_2 are much smaller than ($j\omega L_m$ + R_m). The mode switch part consists of a voltage-controlled low dropout regulator (LDO) module and MOSFET Q_3 and Q_4.

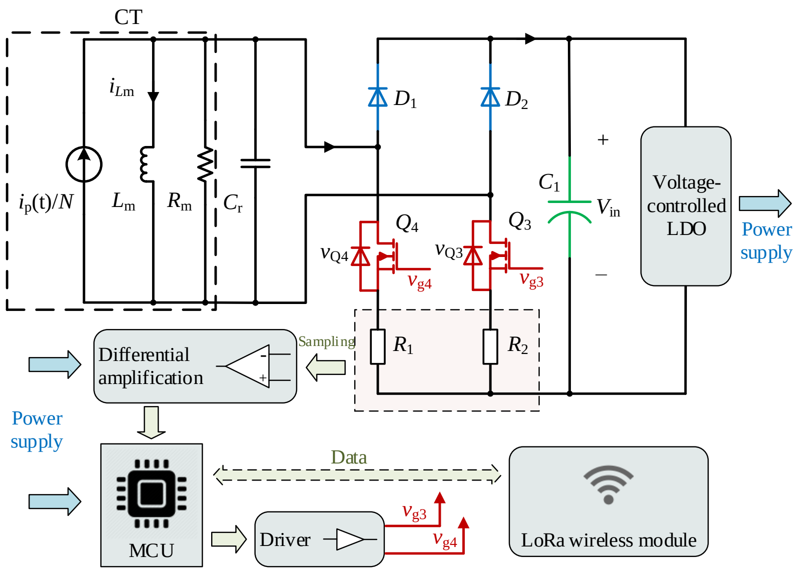

Figure 8. Detailed circuit of the time-multiplexed self-powered wireless current sensor.

3.2. Mode Switch and System Workflow

The mode switch is controlled by the voltage-controlled LDO module. The structure of the voltage-controlled LDO module is shown in Figure 9. The module consists of an LDO with a turned-off state and periphery circuits. The LDO has an enable pin EN, which can control the operating state of the device. When the EN pin voltage is lower than a certain threshold voltage (set as V_{EN_off}), the LDO operates in the turned-off state, where the LDO output voltage is 0. When the EN pin voltage is higher than a certain threshold voltage (set as V_{EN_on}), the LDO operates in a turned-on state, where the LDO outputs a constant voltage. The voltage of the EN pin when the LDO operates in the turned-off state is:

$$V_{EN} = V_{in} \cdot \frac{R_4 \parallel R_5}{R_1 + R_4 \parallel R_5} \tag{12}$$

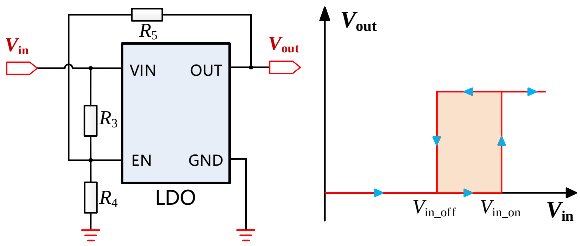

Figure 9. Voltage-controlled LDO module and its input/output characteristics.

The voltage of the EN pin when the LDO operates in the turned-on state is:

$$V_{\mathrm{EN}} = V_{\mathrm{in}} \cdot \frac{R_4 \parallel R_5}{R_1 + R_4 \parallel R_5} + V_{\mathrm{out}} \cdot \frac{R_3 \parallel R_4}{R_5 + R_3 \parallel R_4} \tag{13}$$

Since the output voltage of LDO is constant in the turned-on state (set as $V_{\mathrm{out\_std}}$), thus, at turned-on critical point and turned-off critical point, the voltage of the EN pin is:

$$V_{\mathrm{EN\_on}} = V_{\mathrm{in\_on}} \cdot \frac{R_4 \parallel R_5}{R_1 + R_4 \parallel R_5} \tag{14}$$

$$V_{\mathrm{EN\_off}} = V_{\mathrm{in\_off}} \cdot \frac{R_4 \parallel R_5}{R_1 + R_4 \parallel R_5} + V_{\mathrm{out\_std}} \cdot \frac{R_3 \parallel R_4}{R_5 + R_3 \parallel R_4} \tag{15}$$

Thus, through the peripheral circuit design, the LDO can be turned on when the input voltage is higher than $V_{\mathrm{in\_on}}$, and be turned off when the input voltage is lower than $V_{\mathrm{in\_off}}$, as shown in Figure 9. $V_{\mathrm{in\_on}}$ and $V_{\mathrm{in\_off}}$ are easy to be calculated as:

$$V_{\mathrm{in\_on}} = V_{\mathrm{EN\_on}} \cdot \frac{R_1 + R_4 \parallel R_5}{R_4 \parallel R_5} \tag{16}$$

$$V_{\mathrm{in\_off}} = \left(V_{\mathrm{EN\_off}} - V_{\mathrm{out\_std}} \cdot \frac{R_3 \parallel R_4}{R_5 + R_3 \parallel R_4} \right) \cdot \frac{R_1 + R_4 \parallel R_5}{R_4 \parallel R_5} \tag{17}$$

Based on the above analysis, the workflow of the system is presented, as shown in Figure 10. In the beginning, the voltage of C_1 (V_{in}) is 0, the voltage-controlled LDO is turned off and the MCU is powered off, hence, the Q_3 and Q_4 are turned off. The system operates in energy harvesting mode. The equivalent circuit is shown in Figure 11. The CT with capacitance compensation sources energy from the transmission line. The full-bridge rectifier composed of diodes D_1, D_2, and body diodes of Q_3 and Q_4 converts the AC power on the secondary side of CT to DC power, and stores the energy in C_1. When the voltage of C_1 reaches $V_{\mathrm{in\_on}}$, the voltage-controlled LDO is turned on and the MCU is powered. The MCU starts to operate and turns Q_3 and Q_4 on. At this point, the system is switched to the current measurement mode. The equivalent circuit is shown in Figure 12. Since R_1 and R_2 are much smaller than ($j\omega L_{\mathrm{m}}$ + R_{m}), the current through R_1 and R_2 follows Equation (1). The voltage values of R_1 and R_2 are sensed and entered into the ADC sampling pin of MCU after differential amplification. The current value of R_1 and R_2 is calculated by MCU, and the transmission line current is further calculated according to Equation (1). Finally, the results are sent via the wireless communication module to realize the further function. With energy consumption, the V_{in} drops until it reaches $V_{\mathrm{in\_off}}$, then the voltage-controlled LDO is turned off. The MCU is out of power and the Q_3 and Q_4 are turned off. Then the system re-enters the energy harvesting mode, and the cycle repeats. In a time-multiplexed cycle, the energy consumed by the sensor is:

$$W = \frac{1}{2} C_1 \cdot \left(V^2{}_{\mathrm{in\_on}} - V^2{}_{\mathrm{in\_off}} \right) \tag{18}$$

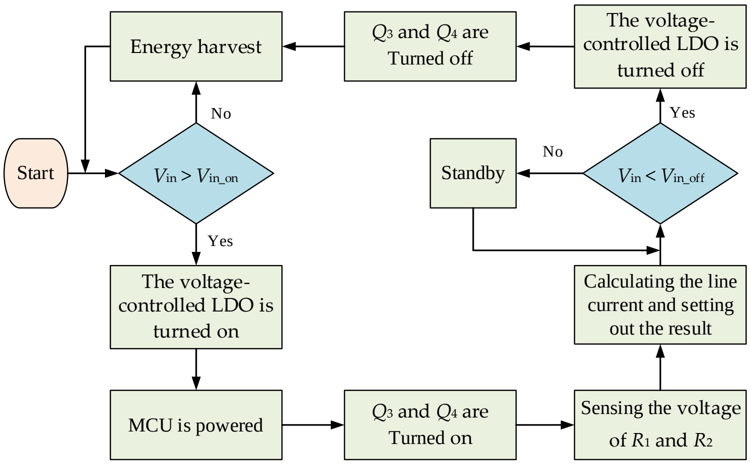

Figure 10. The workflow of the system.

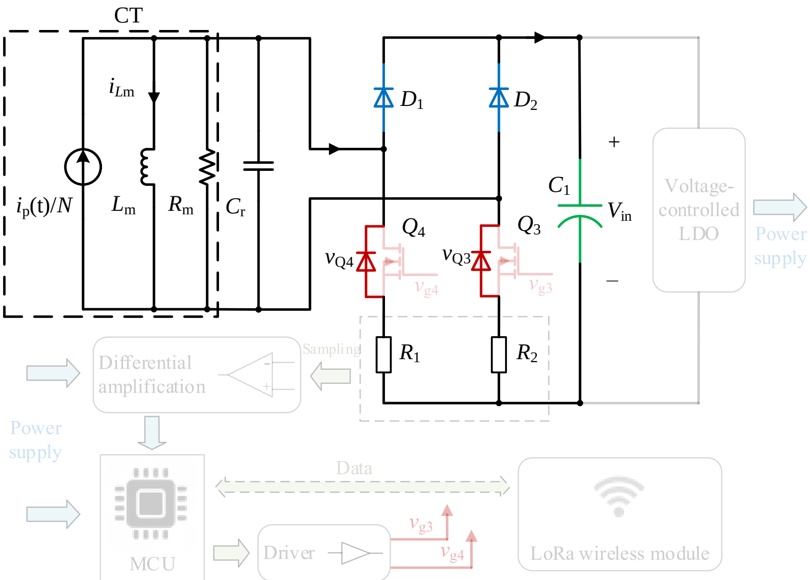

Figure 11. The equivalent circuit of the system operating in energy harvesting mode.

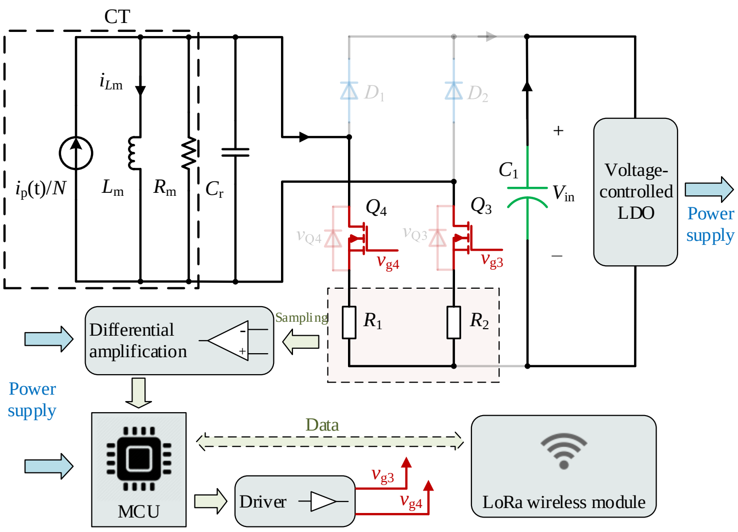

Figure 12. The equivalent circuit of the system operating in current measurement mode.

To verify the operation of the proposed time-multiplexed self-powered current sensor, the circuit is simulated by the PSIM 9 circuit simulation tool. The system parameters in the simulation are consistent with those of the prototype, as shown in Table 1. The simulation results are shown in Figure 13. The time interval between each time the system enters the measurement mode varies with the transmission line current. In other words, the operating frequency of the sensor is limited by the transmission line current. The larger the transmission line current, the higher the operating frequency of the sensor.

Table 1. Parameters of the prototype.

Symbol	Parameter	Value
L_m	CT's excitation inductance	27.5 H
-	CT's airgap	0.1 mm
N	Turns of CT secondary side	4000
C_r	Compensation capacitor	368 nF
C_1	Energy storage capacitor	1 mF
R_1R_2	Sampling resistance	2 Ω
Q_3Q_4	MOSFET	FDS6990AS
D_1D_2	Schottky diode	SD1206S040S2R0
LDO	-	SP6201EM5-L-3-3
V_{in_on}	-	4.8 V
V_{in_off}	-	3.3 V

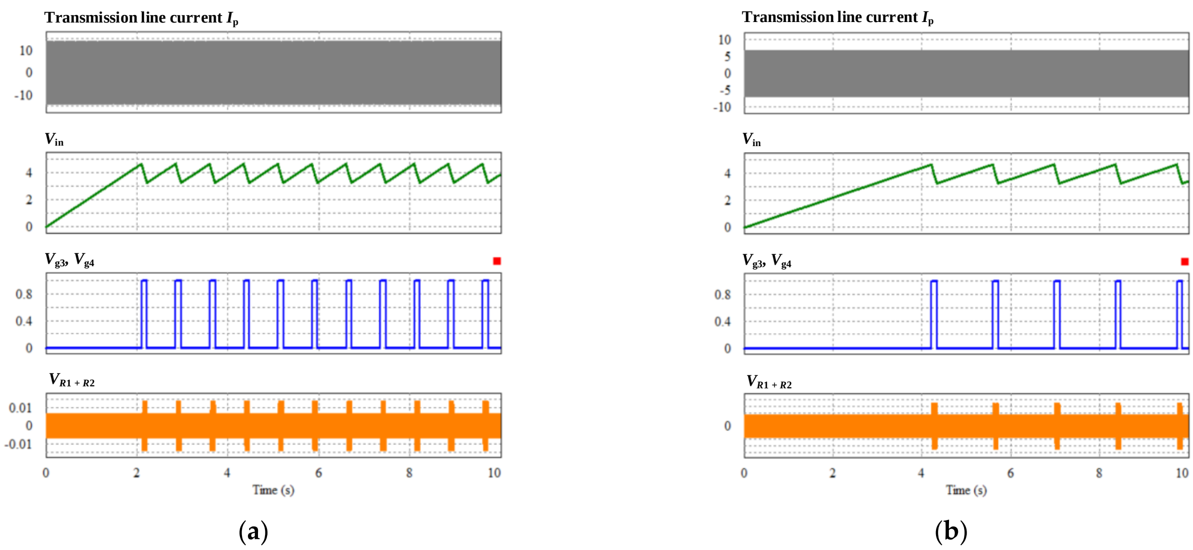

Figure 13. The simulation results of the proposed sensor. (**a**) The transmission line current is 10 A. (**b**) The transmission line current is 5 A.

3.3. Wireless Communication Module

Considering the geographical environment of transmission lines, wireless communication is the best alternative to exchange data with the sensor. LoRa is a long-range, low-power, low-bitrate, wireless telecommunications system, promoted as an infrastructure solution for the Internet of Things [22]. LoRa is very suitable for the application of the proposed sensor, for the low power consumption can improve the operating frequency of the sensor, and the long communication distance can effectively minimize the number of sensors in unit space. The wireless communication module adopts an efficient ISM Band RF spread spectrum chip sx1278. The operating frequency of the module is 410–441 MHz, receiving sensitivity is up to −136 dBm, transmitting distance is 3km, and minimum transmission power is less than 10 mW.

4. Experimental Verification

A test bench is built to demonstrate the proposed current sensor, as shown in Figure 14a. It includes a programmable AC source with a maximum output current of 20 A (50 Hz), a sliding rheostat as AC resistor load, and an oscilloscope. The output of the AC source is used to simulate the transmission line on the primary side of CT. To achieve an equivalent of 100 A maximum primary current, 5 turns are wound on the CT primary side. The prototype of the proposed sensor is shown in Figure 14b. A Cortex-M4 microcontroller STM32F407 is used for controlling and sampling. The prototype parameters are listed in Table 1.

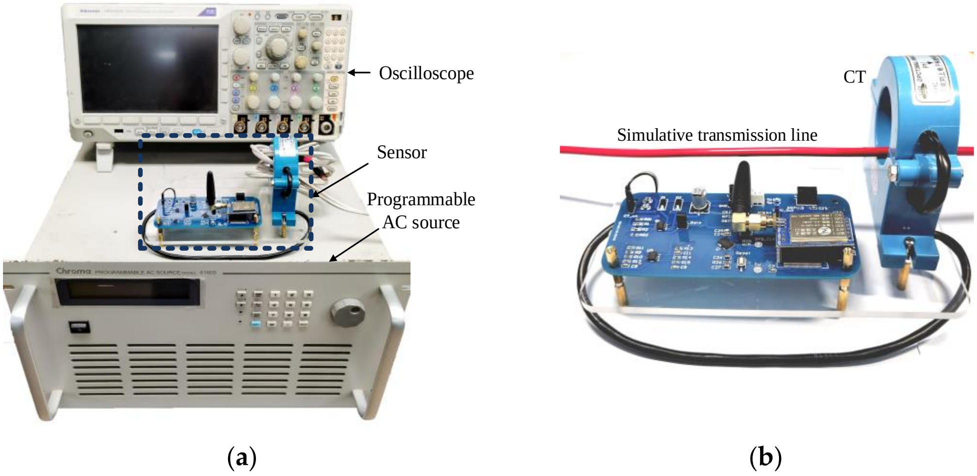

Figure 14. (**a**) Test bench for proposed sensor. (**b**) Prototype of the proposed current sensor.

The functions of the proposed sensor and the accuracy of measurement are verified by experiments. The programmable AC source generates standard sinusoidal signals with different amplitudes to simulate transmission line current. Through the oscilloscope, the operating condition of each part of the circuit can be observed, and the accuracy of current measurement can be evaluated by the data transmitted via the wireless communication module and received by an upper computer.

The experimental waveform of the prototype is shown in Figure 15, the primary side current is set to 5 A (Channel 1). The time intervals of the two patterns in Figure 15 represent two operating modes. It can be seen that the sensor is operating alternatively in energy harvesting mode and current measurement mode. In the energy harvesting mode, the voltage of the energy storage capacitor C_1 (Channel 2) keeps rising until it reaches $V_{\mathrm{in\_on}}$ (4.8 V). Then the system enters the current measurement mode. It can be seen from the enlarged view that in the current measurement mode, the output voltage of the LDO (Channel 3) is 3.3 V, which powers other modules. The ADC sampling pin signal (Channel 4) is a sine wave with DC offset, the phase lags the primary current by 90 degrees, and the amplitude of the sine wave is directly proportional to the CT primary side current value. After sensing the amplitude value of the sine wave, the MCU calculates the current value of the CT primary side and sends out the results. In the current measurement mode, energy is continuously consumed and the voltage of C_1 drops until it reaches $V_{\mathrm{in\_off}}$ (3.3 V), then the system re-enters the energy harvesting mode, the next cycle begins. The power the measurement module requires while it is operating is 50.4 mW. The period of the time-multiplexed cycle is about 1.06 s, and the average power consumption of the sensor estimated by Equation (18) is 5.7 mW.

The sensor works in time-multiplexed mode, the working frequency of the sensor varies with the transmission line current. The time interval between the measurements against the transmission line current is shown in Figure 16. It can be seen that the time interval reducing as the line current increases. By extending the time interval, the sensor can adapt itself to a minimum line current of 1 A, at the expense of a low operating frequency. In this condition, the average power consumption of the sensor is 0.84 mW.

Each time the sensor enters the current measurement mode, the upper computer can receive the data sent by the LoRa wireless communication module of the sensor. The data is the measured primary current value, which is calculated by the MCU. The actual current values and the measured results are shown in Table 2.

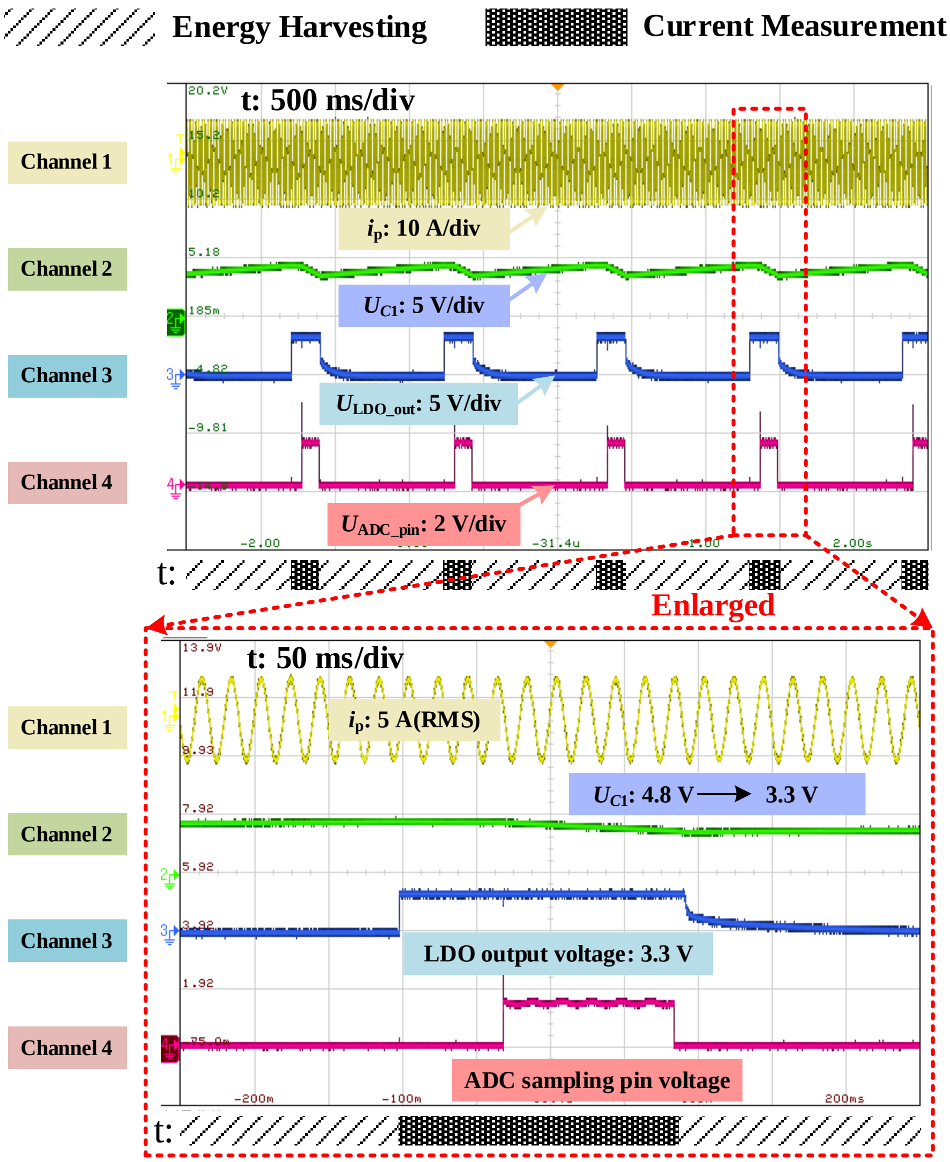

Figure 15. Time-multiplexed waveform of the prototype.

The experimental current measurement range of the sensor is 1–100 A. In Table 2, the actual value is the constant current output of the AC source. The measured value is the current value calculated by the sensor. To reduce the deviation caused by the tolerance of components, linear fitting of data is carried out by using OriginPro (OriginLab, Northhampton MA, USA). The measured values and the actual values are used for the linear fitting. The empirical expression and the correlation factor are:

$$\begin{cases} y = 1.0121x - 0.076 \\ R^2 = 0.99997 \end{cases} \quad (19)$$

The equation represents that the measured current value (i.e., the fitted value) obtained by the device is x when the actual current value is y. The error in Table 2 is the difference between the fitted value and the actual value. And a total range (100 A) is the basis for estimating the errors. Therefore, the error in Table 2 is the absolute error over the max current range. It can be seen that, within the designed current measurement range, the absolute error is within 0.5%, which demonstrates the current measurement accuracy of the proposed time-multiplexed self-powered wireless current sensor. For the parameters of the measurement circuit and the specification of CT are designed for the maximum current measurement range of 100 A, the relative error at low current is relatively high, which is the content that needs further optimization in the future. Table 3 summarizes the performance of the self-powered current sensor in comparison with the previous literature. Compared to the previous CT-fed current sensor [15,16,18], the proposed sensor can work under lower line current and achieve smaller measurement error and shorter measurement interval.

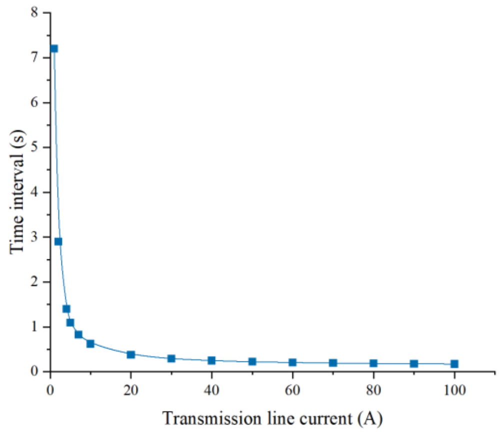

Figure 16. The time interval between the measurements against the transmission line current.

Table 2. Calculated primary side current (unit: A).

Actual Value	Measured Value	Fitted Value	Error (Error/Total Range)	Time Interval per Measurement (s)
1	0.92	0.85	0.15%	7.2
5	4.98	4.96	0.04%	1.06
10	9.87	9.91	0.09%	0.62
20	19.94	20.10	0.10%	0.37
30	29.84	30.12	0.12%	0.29
40	39.73	40.14	0.14%	0.25
50	49.63	50.16	0.16%	0.22
60	59.39	60.03	0.03%	0.21
80	78.76	79.64	0.36%	0.19
100	98.98	100.10	0.10%	0.18

Table 3. Performance comparison.

Literature	Minimum Operating Current	Number of CT Secondary Coils	Measuring Error	Measurement Interval (line Current: 10 A)
[16], Year 2019	20 A	1	<2.5%	-
[18], Year 2019	5 A	2	Not mentioned	8 s
[15], Year 2015	0.8 A	1	<10%	>60 s
This work	1 A	1	<0.5%	0.62 s

5. Conclusions

In this paper, a time-multiplexed self-powered wireless current sensor for power transmission lines is proposed and demonstrated. Two operating modes of CT, including the current sensing mode and the energy harvesting mode, are analyzed in detail. The current sensing function and the energy harvesting function of CT are integrated, the sensor can be self-powered while measuring line current. The mode-switching circuit is designed to isolate the harvesting circuit and the measurement circuit, which eliminates the interference between energy harvesting and current measurement. The accurate current measurement and the maximum energy collection are realized through only one CT secondary coil instead of two coils, which simplifies the design of OCMS. The designed time-multiplexed working mode allows the sensor to work at a lower transmission line current, at the expense of a lower operating frequency. The functions of the proposed sensor are verified by the experiment. The experimental results demonstrate that the sensor can work at a minimum line current of 1 A with 0.84 mW power consumption. And when the transmission line current is within the range of 1 A–100 A, the proposed sensor can operate and measure line current stably. Compared to the previous CT-fed current sensor, the proposed sensor can work under a lower transmission line current and achieve smaller measurement error and shorter measurement interval.

Author Contributions: Conceptualization, H.C. and J.W.; data curation, H.C.; software, C.L.; validation, H.C. and Z.Q.; formal analysis, H.C.; investigation, H.C. and Z.Q.; writing—original draft preparation, H.C.; writing—review and editing, H.C., Z.Q. and J.W.; visualization, C.L.; supervision, J.W., W.L. and X.H.; funding acquisition, X.H. All authors have read and agreed to the published version of the manuscript.

Funding: This research was funded in part by the National Key Research and Development Program of China under Grant 2017YFE0112400 and in part by the National Natural Science Foundation of China, under Grant U1834205.

Institutional Review Board Statement: Not applicable.

Informed Consent Statement: Not applicable.

Data Availability Statement: Not applicable.

Conflicts of Interest: The authors declare no conflict of interest.

References

1. Guo, C.; Dong, M.; Yang, X.; Wang, W. A Review of On-line Condition Monitoring in Power System. In Proceedings of the 2019 IEEE 8th International Conference on Advanced Power System Automation and Protection (APAP), Xi'an, China, 21–24 October 2019; pp. 634–637.
2. Huo, Y.; Prasad, G.; Atanackovic, L.; Lampe, L.; Leung, V.C.M. Cable Diagnostics with Power Line Modems for Smart Grid Monitoring. *IEEE Access* **2019**, *7*, 60206–60220. [CrossRef]
3. Dehghanian, P.; Guan, Y.; Kezunovic, M. Real-Time Life-Cycle Assessment of High-Voltage Circuit Breakers for Maintenance Using Online Condition Monitoring Data. *IEEE Trans. Ind. Appl.* **2019**, *55*, 1135–1146. [CrossRef]
4. Bhattarai, B.P.; Gentle, J.P.; Hill, P.; McJunkin, T.; Myers, K.S.; Abbound, A.; Renwick, R.; Hengst, D. Transmission line ampacity improvements of altalink wind plant overhead tie-lines using weather-based dynamic line rating. In Proceedings of the 2017 IEEE Power & Energy Society General Meeting, Chicago, IL, USA, 16–20 July 2017; pp. 1–5. [CrossRef]
5. Panteli, M.; Kirschen, D.S. Situation awareness in power systems: Theory, challenges and applications. *Electr. Power Syst. Res.* **2015**, *122*, 140–151. [CrossRef]
6. Rivas, A.E.L.; Da Silva, N.; Abrão, T. Adaptive current harmonic estimation under fault conditions for smart grid systems. *Electr. Power Syst. Res.* **2020**, *183*, 106276. [CrossRef]
7. Wang, Z.; Hu, J.; Ouyang, Y.; Deng, Y.; Zhao, G.; He, J.; Wang, S.X. A self-sustained current sensor for smart grid application. *IEEE Trans. Ind. Electron.* **2020**, 1. [CrossRef]
8. Ray, W.; Hewson, C. High performance Rogowski current transducers. In Proceedings of the Conference Record of the 2000 IEEE Industry Applications Conference. Thirty-Fifth IAS Annual Meeting and World Conference on Industrial Applications of Electrical Energy (Cat. No.00CH37129), Rome, Italy, 8–12 October 2000; Volume 5, pp. 3083–3090.
9. Chen, K.-L.; Tsai, Y.-P.; Chen, N. Design of a Novel Power Current Micro-Sensor for Traction Power Supply Using Two Hall ICs. In Proceedings of the 2009 IEEE 70th Vehicular Technology Conference Fall, Anchorage, AK, USA, 20–23 September 2009; pp. 1–5.

10. Michie, W.; Cruden, A.; Niewczas, P.; Madden, W.; McDonald, J.; Gauduin, M. Harmonic analysis of current waveforms using optical current sensor. *IEEE Trans. Instrum. Meas.* **2002**, *51*, 1023–1026. [CrossRef]
11. Kishore, R.A.; Priya, S. A Review on Low-Grade Thermal Energy Harvesting: Materials, Methods and Devices. *Materials* **2018**, *11*, 1433. [CrossRef] [PubMed]
12. Wang, C.; Li, J.; Yang, Y.; Ye, F. Combining Solar Energy Harvesting with Wireless Charging for Hybrid Wireless Sensor Networks. *IEEE Trans. Mob. Comput.* **2017**, *17*, 560–576. [CrossRef]
13. Tan, Y.K.; Panda, S.K. Optimized Wind Energy Harvesting System Using Resistance Emulator and Active Rectifier for Wireless Sensor Nodes. *IEEE Trans. Power Electron.* **2010**, *26*, 38–50. [CrossRef]
14. Qian, Z.; Wu, J.; He, X.; Lin, Z. Power Maximized and Anti-Saturation Power Conditioning Circuit for Current Transformer Harvester on Overhead Lines. *IET Power Electron.* **2018**, *11*, 14, 2271–2278. [CrossRef]
15. Amaro, J.P.; Cortesão, R.; Landeck, J.; Ferreira, F.J.T.E. Harvested Power Wireless Sensor Network Solution for Disaggregated Current Estimation in Large Buildings. *IEEE Trans. Instrum. Meas.* **2015**, *64*, 1. [CrossRef]
16. Ren, J.; Sun, Y.; Zhang, S.; Zhang, S.; Liu, Y.; Li, K.; Jiang, X. A Novel Self-Powered Smart Current Sensor for Power Equipment. *Elektron. Elektrotechnika* **2019**, *25*, 20–27. [CrossRef]
17. Moghe, R.; Lambert, F.C.; Divan, D. Smart "Stick-on" Sensors for the Smart Grid. *IEEE Trans. Smart Grid* **2011**, *3*, 241–252. [CrossRef]
18. Lim, T.; Kim, Y. Compact Self-Powered Wireless Sensors for Real-Time Monitoring of Power Lines. *J. Electr. Eng. Technol.* **2019**, *14*, 1321–1326. [CrossRef]
19. Krieger, E.M.; Cannarella, J.; Arnold, C.B. A comparison of lead-acid and lithium-based battery behavior and capacity fade in off-grid renewable charging applications. *Energy* **2013**, *60*, 492–500. [CrossRef]
20. Miller, J.R. Perspective on electrochemical capacitor energy storage. *Appl. Surf. Sci.* **2018**, *460*, 3–7. [CrossRef]
21. Li, Y.; Liu, Q.; Hu, S.; Liu, F.; Cao, Y.; Luo, L.; Rehtanz, C. A Virtual Impedance Comprehensive Control Strategy for the Controllably Inductive Power Filtering System. *IEEE Trans. Power Electron.* **2016**, *32*, 920–926. [CrossRef]
22. Augustin, A.; Yi, J.; Clausen, T.; Townsley, W.M. A Study of LoRa: Long Range & Low Power Networks for the Internet of Things. *Sensors* **2016**, *16*, 1466. [CrossRef]